Naval Command,
Control and Ocean
Surveillance Center RDT&E Division San Diego, CA
92152-5000

Technical Report 1480
March 1992

Feasibility of a 486 nm Fraunhofer Laser Source Based on a $^4F_{3/2} \rightarrow {}^4I_{9/2}$ Neodymium Laser

F. E. Hanson
D. L. Katz
P. Poirier

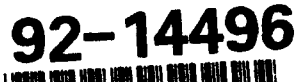

Technical Report 1480
March 1992

Feasibility of a 486 nm Fraunhofer Laser Source Based on a $^4F_{3/2} \rightarrow {}^4I_{9/2}$ Neodymium Laser

F. E. Hanson
D. L. Katz
P. Poirier

NAVAL COMMAND, CONTROL AND OCEAN SURVEILLANCE CENTER
RDT&E DIVISION
San Diego, California 92152-5000

J. D. FONTANA, CAPT, USN
Commanding Officer

R. T. SHEARER
Executive Director

ADMINISTRATIVE INFORMATION

This work was performed by Code 843, RTD&E Division of the Naval Command, Control and Ocean Surveillance Center.

Released by
D. M. Gookin, Head
Electro-Optic Devices
Branch

Under authority of
M. S. Kvigne, Head
Satellite Communications
Division

JT

EXECUTIVE SUMMARY

OBJECTIVE

Investigate the potential of a novel laser source based on the neodymium $^4F_{3/2} \rightarrow {}^4I_{9/2}$ transition for operation at 486.1 nm, the H_β Fraunhofer wavelength. Characterize this transition in Nd:YAG and also stimulated rotational Raman conversion in H_2, D_2, and HD as critical steps in such a system.

RESULT

The efficiency of Nd:YAG at 946 nm is not inherently low, however, major efforts would be required to solve or reduce the problems. The output at 946 nm was found significantly limited at near ambient temperatures due to ASE losses at the high gain 1064 nm transition. Single pass rotational Raman conversion efficiencies of 65 to 80 percent were measured at 532 nm for the three hydrogen isotopes.

CONCLUSIONS

We should be able to demonstrate an efficient and scalable Nd:YAG laser source at 946 nm, however some means of reducing the ASE loss at 1.06 μm must be found. Ideally, a 1.06-μm absorber would be codoped into the crystal host to reduce the gain. Another method would be to segment the active media with filters to block the 1.06 μm and also pass 0.946 μm with high efficiency.

Raman conversion has been efficiently demonstrated in all three hydrogen isotopes. In a space environment it should also be practical to operate a Raman cell at low temperature since only a small fraction of laser power is dissipated in the gas. Three of the systems identified in table 1 require a J=0->2 transition and would be possible at lower temperatures.

INTRODUCTION

There is a considerable interest in finding an efficient and long-lived laser/receiver system for covert optical communication in the ocean environment. A major problem with this technology is finding a suitable laser source with the appropriate wavelength to match up with the best filter/receiver candidates in the blue-green spectral region where the transmission in seawater is peaked. The cesium atomic-resonance filter at 455 and 459 nm has received the most attention to date. This filter has a very narrow bandwidth, an isotropic field of view, and has demonstrated high-quantum efficiency. However, a simple efficient laser source at these wavelengths does not exist. The best candidates are considered to be the XeCl excimer laser with Raman shifting in hot lead vapor (Rieger, 1986), a frequency tripled Nd:YALO laser with rotational Raman shifting in D_2 or H_2 (Bowman, et al., 1989), or a frequency doubled Nd:YAG laser pumping a Ti:Sapphire laser with the infrared output either frequency doubled or mixed with 1.06 μm from the Nd:YAG (Brown, et al., 1991). All of these approaches are complex and require careful frequency control to maintain the precise wavelength that is somewhat off the wavelength of the free-running laser. In addition, if the transmitter satellite is in a low-earth orbit, the laser would require some degree of wavelength control to compensate for a Doppler shift relative to the receiver.

Alternatively, Lyot type filters can be designed to operate throughout the blue-green region. These filters generally tradeoff bandwidth with angular acceptance and the operating bandwidth would not be expected to be as narrow as a filter based on atomic transitions. However, if such a filter is combined with the broad Fraunhofer dip in the solar background at 486.13 nm (H_β line) (Beckers et al., 1976), a noise reduction of ~4 can be achieved relative to the continuum. Figure 1 shows the FWHM of this dip is more than 1 A, and the wavelength requirements of a laser source here would not be as severe as the case with an atomic-resonance filter.

Laser diode pumped solid-state lasers have been widely demonstrated in the last few years to exhibit efficiencies and lifetimes that are substantially improved over comparable flashlamp pumped lasers. On the other hand, electric discharge pumped excimer lasers have not been widely used in the military environment due to their engineering complexity. It seems clear that diode pumped laser systems will become increasingly important in many military and commercial applications. Unfortunately, apart from two-photon upconversion lasers (Nguyen, et al., 1990; MacFarlane, 1991), there are no diode pumped solid-state lasers that operate directly in the blue-green spectral region. Second harmonic generation of the strong 1.06-μm transition in neodymium gives 532 nm which can be very useful, but is outside the optimum wavelength region for underwater transmission.

Operation on the lower gain $^4F_{3/2} \rightarrow {}^4I_{9/2}$ transition in neodymium is also possible and would allow direct frequency doubling to the blue. Figure 2 shows the range of laser wavelengths obtained from each of the $^4F_{3/2}$ levels to the upper $^4I_{9/2}$ level from published data for a large sample of different neodymium doped laser materials (Kaminskii, 1981). Generally, as the crystal field splitting of the ground state increases, the wavelength increases as might be expected. Clearly, the number of different oxide host materials is much larger than the number of fluorides because of the two bond coordination of oxygen. The wavelength of this transition in the oxides also tends to be slightly longer for a given ground state splitting. In all these materials, the terminal laser level is only a few hundred cm^{-1} above the ground-state, and there can be significant thermal population and therefore absorption at the laser wavelength. Some specific wavelengths of interest are at twice the cesium resonances and at twice the Fraunhofer H_β absorption dip, 911, 919, and 972 nm respectively. There are a number of possible 911-nm materials, however the ground state absorption is prohibitive except at cryogenic temperatures (Hanson, et al., 1991). There are no known hosts with sufficient crystal field to give emission at 972 nm.

The approach investigated in this project was to begin with a neodymium laser operating at the longer wavelength end of the $^4F_{3/2} \rightarrow {}^4I_{9/2}$ range and use a combination of frequency doubling and Raman shifting to reach 486 nm. Several laser-host materials were identified where the resultant output would be reasonably close to the H_β-Fraunhofer line. Table 1 lists some of the possible laser- and Raman-shift systems. The second and third columns show the splitting of the terminal-laser level above the ground state and the laser wavelength respectively. The appropriate Raman medium is identified and the Raman shift is given. The process is either a Raman shift followed by frequency doubling or the reverse. Finally, the wavelength tuning required to exactly match the Fraunhofer dip is given. This dip is the wavelength error in the infrared from the free-running laser output; the wavelength error for the blue output would be about half of this value. The laser-tuning range for neodymium could probably extend over a few angstroms in most of these materials.

The class of garnet-crystal hosts, given by the generic formula $A_3B_5O_{12}$ and typified by $Y_3Al_5O_{12}$ or YAG, allows a broad range of atomic substitution. A number of garnets are represented in figure 2 where we see that the garnets have some of the largest ground-state splittings. There is a good possibility that additional garnet materials could be found that would give an even better match to the desired Fraunhofer wavelength. However, the first step in the entire process is the demonstration of an efficient Q-switched laser operating on this transition. Our first objective was to characterize the Nd:YAG laser at 946 nm even though this output is 0.9 nm too long for the process identified in table 1. The problems encountered with this laser would be similar, and probably worse, in the other systems.

Table 1. Possible two-step nonlinear approaches to reach 486.1 nm based on a neodymium $^4F_{3/2}$ – $^4I_{9/2}$ laser. The process x2,R gives $2\omega_L - \omega_R$ and R,x2, gives $2(\omega_L - \omega_R)$.

Crystal Host	$\Delta E - {}^4I_{9/2}$ (cm^{-1})	λ(nm)	Raman Medium	ω_R(cm^{-1})	Process	$\Delta\lambda$(nm)
$LuAlO_3$	662	931.9	HD (1→3)	444.9	R,x2	0
$Gd_3Sc_2Al_3O_{12}$	808	942.2	CS_2	658	x2,R	0.1
$Lu_3Sc_2Al_3O_{12}$	808	942.2	CS_2	658	x2,R	0.1
$YScO_3$	709	955.5	D_2 (0→2)	179	R,x2	-0.1
$Lu_3Al_5O_{12}$	878	941.3	CH_3Cl	674	x2,R	-0.1
$Lu_3Al_5O_{12}$	878	947.3	HD (0→2)	267.3	R,x2	-0.3
$Y_3Al_5O_{12}$	857	946.1	H_2 (1→3)	590	x2,R	0.9
CaMgYGeO	807	939.7	H_2 (0→2)	354	R,x2	-0.2
$Y_3Sc_2Ga_3O_{12}$	778	938.0	NO_2	750	x2,R	0.0
$Lu_3Ga_5O_{12}$	777	937.6	NO_2	750	x2,R	-0.4

Relatively high efficiencies with Nd:YAG have been achieved at room temperature in low-power experiments at 946 nm by using small crystal lengths to limit the ground-state absorption (Fan and Byer, 1987). In diode-pumped experiments with a 1-cm Nd:YAG rod, 17 percent optical slope efficiency has been demonstrated at a temperature of -40°C (Hays and Burnham, 1990). With flashlamp pumping of a 3-inch 1-percent Nd:YAG rod in a refrigerated pump cavity at -63.5°C, electrical slope efficiencies of ~0.2 percent have been reported (Rankin et al.). The ground-state absorption (GSA) and laser thresholds are clearly reduced at lower temperatures, however, the required refrigeration energy is a major penalty to overall system efficiency. In this work, we examined lower-doped neodymium rods as a means to achieve the lower thresholds.

In addition, there was a lack of published data on efficient Raman shifting with the listed materials. We know that efficient stimulated rotational Raman scattering (SRRS) can occur in H_2 and D_2 (Bowman, et al., 1989), however experimental details such as gas pressure and pump thresholds are lacking. In this work, we characterized SRRS in H_2, D_2, and HD. Frequency doubling of the ~0.95-μm laser output is not considered a problem and could be achieved using either KDP, BBO, LBO, etc.

NEODYMIUM $^4F_{3/2} \rightarrow {}^4I_{9/2}$ LASER MODELING

There are two considerable problems with laser operation in neodymium between the upper $^4F_{3/2}$ state to the ground $^4I_{9/2}$ state. First, the gain is typically ten times lower than at the strong transition at 1 μm to the $^4I_{11/2}$ state. Second, there can be

significant absorption at the ~0.9-μm laser wavelength due to ground-state population. This absorption results in high-pump thresholds. The laser must be pumped well above threshold to operate efficiently and at the same time parasitic oscillation or amplified spontaneous emission (ASE) at 1 μm must be prevented. The temperature-dependent absorption α in cm^{-1} at 946 nm in Nd:YAG is given by

$$\alpha = N\sigma \frac{e^{-E/kT}}{Z}, \tag{1}$$

where N is the neodymium number density, σ is the cross section of the R1 ↔ Z5 transition, and Z is the partition function of the $^4I_{9/2}$ manifold. We have taken $\sigma = 4 \times 10^{-20}$ in the calculations below (Fan and Byer, 1987). The temperature dependence of α is shown in figure 3 for doping levels of 0.6 and 1 atomic percent, where 1 atomic percent doping corresponds to $N = 1.34 \times 10^{21}$ cm^{-3}. The benefit of the lower doping is apparent: at these temperatures, the ground-state absorption for the lower doping is equivalent to the absorption for the higher doping at a temperature 30 to 40 degrees lower. On the other hand, the pump light will not be absorbed quite as efficiently.

The laser threshold, P_{th}, can be written in terms of the combined cavity losses as

$$P_{th} = \frac{1}{K2L\sigma}[2\alpha L - \ln(R) - \ln(x)], \tag{2}$$

where K is a pumping-efficiency factor relating to the absorption of pump energy in the laser rod, L is the rod length, R is the output mirror reflectivity, and x represents all other factors in the round trip transmission of the laser cavity aside from GSA.

Nd:YAG LASER EXPERIMENTS

Figure 4 shows the experimental configuration. A close-coupled, diffuse-reflecting lamp cavity was placed in a dry nitrogen purged housing and cooled with a water-methanol mixture. For the results discussed below, a 3 inch by 0.25 inch, 0.6 atomic percent Nd:YAG rod was used. All mirrors were flat and chosen to have high transmission at 1.06 μm. Initially a prism was used to discriminate against 1.06-μm lasing, however it was later found that two additional dichroic mirrors placed between the rear high reflector and the laser rod, were sufficient to hold off 1.06 μm in long pulse operation. Three different output couplers were used. Figure 5 shows results with the highest transmission mirror, T = 17.5 percent. The best slope efficiency, 0.42 percent, was achieved with this mirror at 0°C. Figure 6 shows the laser thresholds with different output reflectivities and temperatures. A calculated threshold using equation 1 and 2 and a round-trip cavity transmission of 0.854 is also shown and gives a reasonably good fit to these results. The slope of the fitted lines is 54.1 Joules which corresponds

to $K = 3.0 \times 10^{16}$ ions/Joule-cc in equation 2. Higher values of K would be expected with higher doped laser rods.

Figure 7 shows the slope efficiencies for the same 6 sets of data. For comparison, the slope efficiency obtained at 1.06 μm was ~2 percent. The limiting slope efficiency at 946 nm (with no loss) should in principle be close to this value, however the observed values are about half of what should then be expected.

The explanation for the low-slope efficiencies that we found is that a substantial fraction of the neodymium inversion is lost at higher pump energies due to superradiance at 1.06 μm along the length of the laser rod. We measured the relative gain in the laser rod as a function of lamp energy by measuring the sidelight fluorescence intensity at 939 nm from the end of the rod at ~45 degrees to the rod axis. The fluorescence spectrum was collected with a EG&G reticon detector array which allowed the relatively broad-lamp spectrum to be subtracted from the narrow fluorescence line. The data shown in figure 8 are with all cavity mirrors blocked and clearly shows significant single-pass ASE loss in the laser rod at higher lamp energy. At the highest pump energy, about 40 percent of the extrapolated gain is lost by this process.

STIMULATED ROTATIONAL RAMAN CONVERSION IN H_2, D_2, AND H

A systematic study was made of the relative performance of single-pass stimulated rotational Raman scattering (SRRS) in the three molecular hydrogen isotopes, H_2, D_2, and HD. For these simple diatomics, the energy in cm^{-1} of the rotational level J in the ground vibration state can adequately be represented as (Herzberg, 1950)

$$E_J = hc[B_oJ(J+1) - D_eJ^2(J+1)^2]. \quad (3)$$

Table 2 gives values of the rotational constants. In the homonuclear diatomics H_2 and D_2, two forms, ortho and para, are used to distinguish molecules depending on the total nuclear spin. The ortho form generally refers to the more abundant species and for hydrogen, these are the molecules having a symmetric nuclear-spin function and antisymmetric-rotational functions. Thus, ortho hydrogen can have only odd J values and para hydrogen even J values. For D_2, the opposite is true and the even J states are more common. Transitions between these classes are usually quite slow and require some magnetic perturbation. There are no symmetry restrictions for HD - all J states are equally accessible.

Table 2. Spectroscopic parameters for hydrogen.

Hydrogen Molecule	$B_o(cm^{-1})$	$D_e(cm^{-1})$	I_m	Nuclear degeneracy	J values
H_2	59.32	0.0471	0	1	even
			1	3	odd
D_2	29.90	0.0114	0,2	6	even
			1	3	odd
HD	44.66	0.0261			

Raman transitions J -> J + 2 give rise to different Stokes lines S(J) in the scattered light spectrum on the long wavelength side of the pump. The factors affecting the relative rotational Raman gain at the Stokes wavelength λ_s for the different hydrogen molecules are given by (Rokni and Flushberg, 1986)

$$g = \frac{\Delta N}{\lambda_s \Delta \nu} \frac{(J+1)(J+2)}{(2J+1)(2J+3)}. \tag{4}$$

Scattering is in the forward direction and the generated Stokes wave is circularly polarized opposite to the pump wave. Here ΔN is the temperature-dependent population factor between initial state J_1 and final state J_2

$$\Delta N = N_1 - N_2 \frac{2J_1 + 1}{2J_2 + 1}, \tag{5}$$

and

$$N_J = \frac{\rho}{Z_R} \sum_{I_m} (2I_m + 1)(2J + 1) e^{-E_J/kT}, \tag{6}$$

is the equilibrium population of the J level for a total number density ρ. The summation is over the allowed values of the total nuclear spin I_m, and

$$Z_R = \sum_{I_m, J} (2I_m + 1)(2J + 1) e^{-E_J/kT}, \tag{7}$$

is the rotational partition function.

The linewidth $\Delta\nu$ depends on temperature and density and is, in general, different for each transition in each of the gases. At low density the Raman lineshape is Gaussian due to Doppler broadening. At densities above a critical value, the lineshape is Lorentzian and the linewidth for each transition can be described by a diffusion model (Bischel and Dyer, 1986) where

$$\Delta\nu = A/\rho + B\rho . \quad (8)$$

The critical density is less than 1 amagat ($\sim 2.7 \times 10^{19}$ cc^{-1}) for the first few Stokes lines in H_2 and is expected to be even lower for the heavier isotopes. A minimum linewidth given by $(A/B)^{1/2}$ is the result of collisional narrowing. This occurs for the S(1) line of H_2 at 0.23 amagat.

The gain predicted from equation 5 using this model scales as $\rho/\Delta\nu$ which increases with density and gradually reaches a limiting value at higher density. Above one amagat, the dominate broadening of the first few lines is due to B and is essentially linear in ρ. This coefficient has been measured (Van Den Hout, et al., 1980) for the first few transitions in each of the gases and values are listed in table 3. B is much larger for HD than for either H_2 or D_2. Both A and B have some temperature dependence. For the first three Stokes lines, B decreases by less than 50 percent for H_2 and D_2 and about a factor of 3 for HD from 300 to 77°K. Also, the linear broadening generally decreases with increasing J, however the relative magnitude is less than 50 percent from S(0) to S(3).

Table 3. Collision broadening coefficients, B(MHz m^3/mol).

Gas	S(0)	S(1)	S(2)	S(3)
H_2	0.94	1.17	0.83	0.85
D_2	1.88	1.50	1.39	1.14
HD	9.6	8.5	7.4	6.1

The dominate factor in the gain, $g\Delta\nu/N$, was calculated for the first few rotational lines in each of the three gases in thermal equilibrium as a function of temperature. Figure 9 shows the results at 300K. The S(1) line in H_2 at 588 cm^{-1} is clearly expected to have the largest gain. In D_2 and HD, the largest gain is predicted for S(2) at 415 cm^{-1} and S(1) at 443 cm^{-1}, respectively. Figures 10 through 12 show the temperature dependence of the different lines. At low temperatures, the dominate line will become S(0) for each of the isotopes. This line should happen at ~100°K for H_2 and ~200°K for D_2 and HD.

Figure 13 shows the experimental arrangement used to measure the Raman conversion from a 532-nm pump. Pulses at 10 Hz from a frequency doubled Nd:YAG laser were circularly polarized with a $\lambda/4$ plate and focused near the center of a 1-meter

long gas cell. A beam-splitting plate was placed before the focusing lens and sent a small sample of the pump into an integrating sphere and photodiode detector. This sample was calibrated with a Scientech power meter to give the pulse energy incident on the lens. The cell had flat uncoated windows. All of the light exiting the cell was captured by a second integrating sphere and a fiber-optic bundle brought a sample of the output to a 0.5-meter spectrograph and silicon detector array.

At high-pump energy, and especially with the longer focal length lens, many lines might be observed in the output. The Stokes line $S_1(J)$ with highest gain would reach threshold first and with increasing pump energy, could then, in turn, generate a second order Stokes line $S_2(J)$ at longer wavelength, etc. Also, a vibrational Raman line could usually be observed at some point. The Raman conversion efficiencies described below were effectively the fraction of the pump light at 532 nm that entered the cell and was converted to the first rotational Stokes wavelength $S_1(J)$. The following procedure was used. The wavelength-dependent response of the integrating sphere, fiber optic, and spectrograph was calibrated with a tungsten halogen lamp over a range around the pump wavelength from the first anti-Stokes (AS_1) to a few Stokes orders. A program was written to automatically integrate a number of selected wavelength peaks (e.g., AS_1, P, S_1, S_2) for ~200 pulses at each pump energy. The sum intensity of the selected peaks was found to be linear with pump energy up to a certain level until another process, such as vibrational Raman, began to occur. Sufficient data was taken at low energy to ensure that a good correlation between incident pump energy and peak summation could be made. The conversion efficiency to $S(J)_1$ could then be based entirely on the incident pump energy for all values by using this correlation.

Figures 14 and 15 show the Raman conversion efficiencies $S_1(1)$ at 549 nm for H_2. With a 50-cm focusing lens, a maximum conversion of ~80 percent was obtained for all pressures. As the pressure is increased, the threshold decreases and the maximum conversion occurs at lower pump energy. Higher order $S_n(1)$ processes begin at lower pump energies and cause the $S_1(1)$ efficiency to fall off earlier with increasing pump. This increasing effect was more pronounced with a longer 100-cm focusing lens. Here, a threshold of ~10 mJ was obtained, however the maximum conversion was only ~60 percent.

The results for D_2 and HD are shown in figures 16 and 17 respectively. The gain for these gases was significantly less than for H_2 and a 100-cm focusing lens was used for most of the work. The $S_1(2)$ threshold in D_2 at 544 nm is about half the value for $S_1(1)$ in HD at 545 nm. This is consistent with the much larger linewidth for HD. Maximum conversion was ~75 percent for D_2 and 64 percent for HD.

CONCLUSION

We should be able to demonstrate an efficient and scalable Nd:YAG laser source at 946 nm, however some means of reducing the ASE loss at 1.06 μm must be found. Ideally, a 1.06-μm absorber would be codoped into the crystal host to reduce the gain. Another method would be to segment the active media with filters to block the 1.06 μm and also pass 0.946 μm with high efficiency.

Raman conversion has been efficiently demonstrated in all three hydrogen isotopes. In a space environment, it should also be practical to operate a Raman cell at low temperature since only a small fraction of laser power is dissipated in the gas. Three of the systems identified in table 1 require a J=0->2 transition and would be possible at lower temperatures.

REFERENCES

Beckers, J. M., C. A. Bridges, and L. B. Gilliam. 1976. Air Force Geophysics Lab. report AFGL-TR-76-0126.

Bischel, W. K., and M. J. Dyer. 1986. Phys. Rev. A 33, 3113.

Bowman, S. R., B.J. Feldman, J.M. McMahon, A.P. Bowman, and D.Scarl. 1989. *Tunable Solid State Lasers,* Vol 5 of the OSA proceeding Series, M.L. Shand and H.P. Jensen, eds. Optical Society of America, Washington DC, p. 108.

Brown, A. J. W., K. W. Kangas, and C. H. Fisher. 1991. in *Conference for Lasers and Electro-Optics,* Optical Society of America, Washington, DC, p. 176.

Fan, T. Y., and R. L. Byer. 1987. Opt. Lett. 12, p. 809.

Fan, T. Y., and R. L. Byer. 1987. IEEE J. Quant. Electron. QE-23, 605.

Hanson, D., D. H. Verdun, and M. Kodta. 1991. J. Opt. Soc. Am B 8, p. 1668.

Hays, A. D., and R. Burnham. 1990. *Conference for Lasers and Electro-Optics, 1990* Optical Society of America, Washington, DC, p. 4.

Herzberg. 1950. *Molecular Spectra and Molecular Structure 1. Spectra of Diatomic Molecules,* D. Van Nostrand Company, Princeton, NJ.

Kaminskii, A. A. 1981. *Laser Crystals,* Springer Verlag, NY.

MacFarlane, R. A. 1991. Opt. Lett. 16, p. 1397.

Nguyen, D. C., G. E. Faulkner, M. E. Weber, and M. Dulick. 1990. SPIE 1223 Solid State Lasers p. 54.

Rankin, M. B., G. D. Ferguson, and S. R. Bazow, Naval Air Development Center report NADC-83009-30.

Rieger, H. 1986. IEEE J. Quant. Elect. QE-22, p. 405.

Rokni, M., and A. Flusberg. 1986. IEEE J. Quant. Elect. QE-22, 1102.

Van Den Hout, K. D., P. W. Hermans, E. Mazur, and H. F. P. Knaap. 1980. Physica 104A, 509.

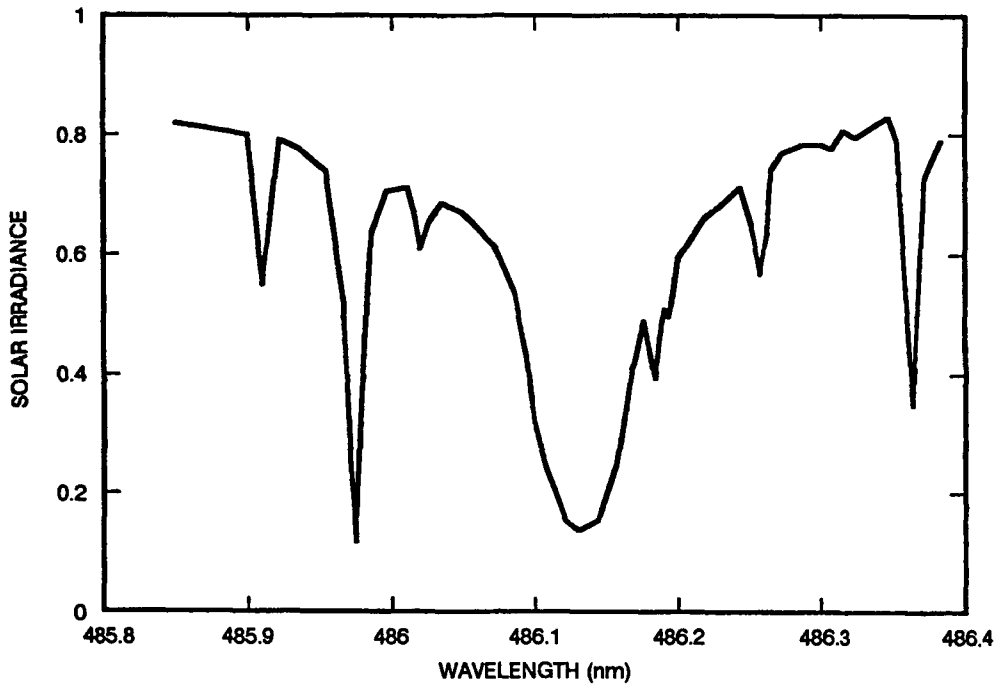

Figure 1. H_β Fraunhofer dip in the solar spectrum.

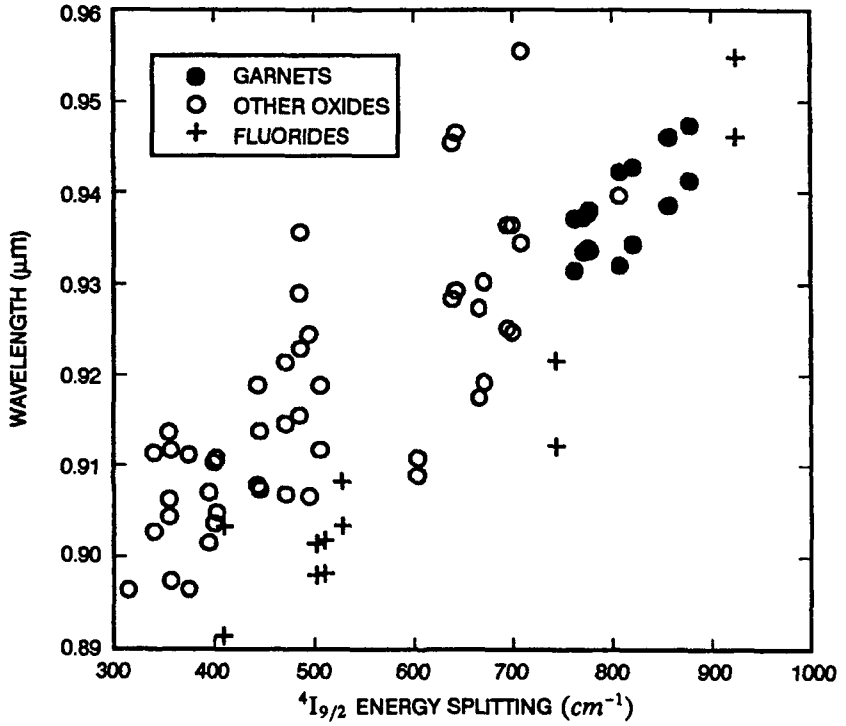

Figure 2. Neodymium emission wavelengths for the $^4F_{3/2}$ levels to the top of the $^4I_{9/2}$ manifold.

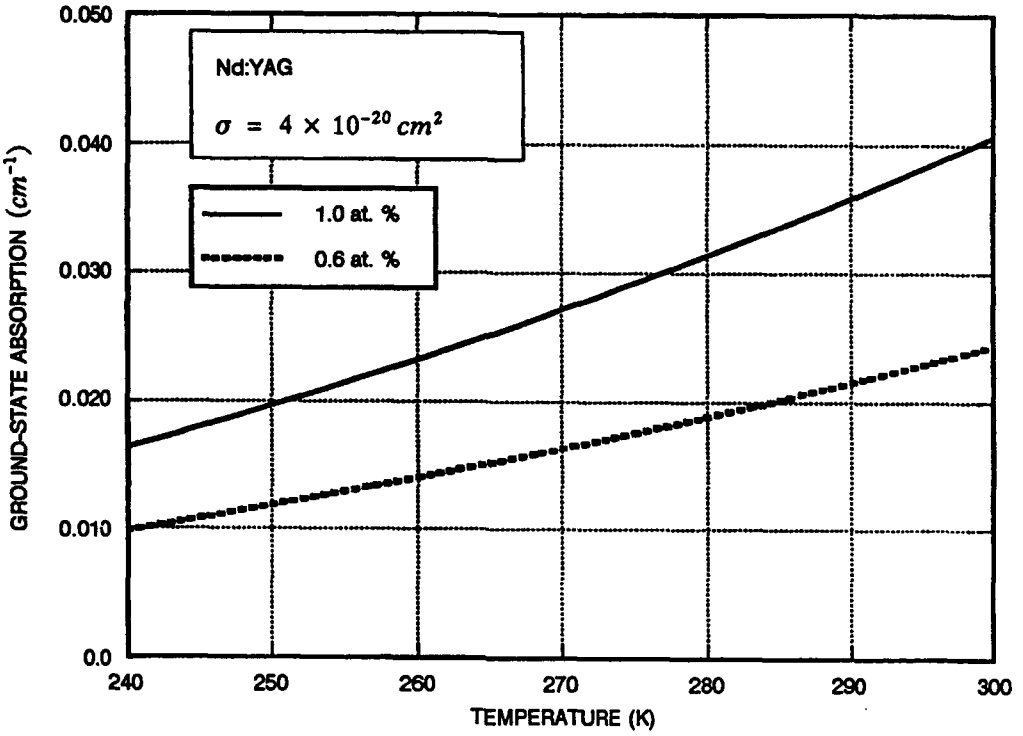

Figure 3. Ground-state absorption in Nd:YAG.

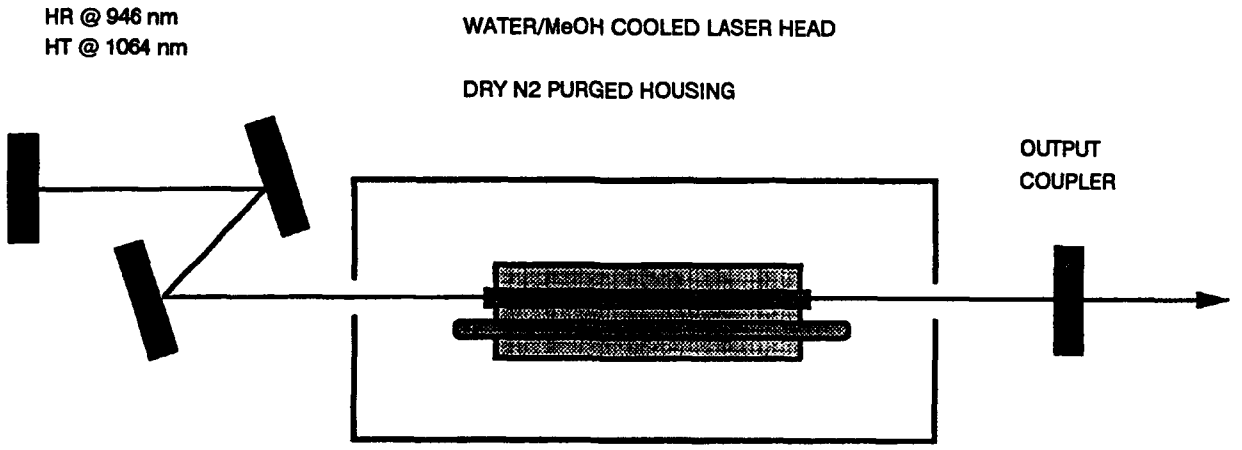

Figure 4. Experimental setup for the 946 nm laser.

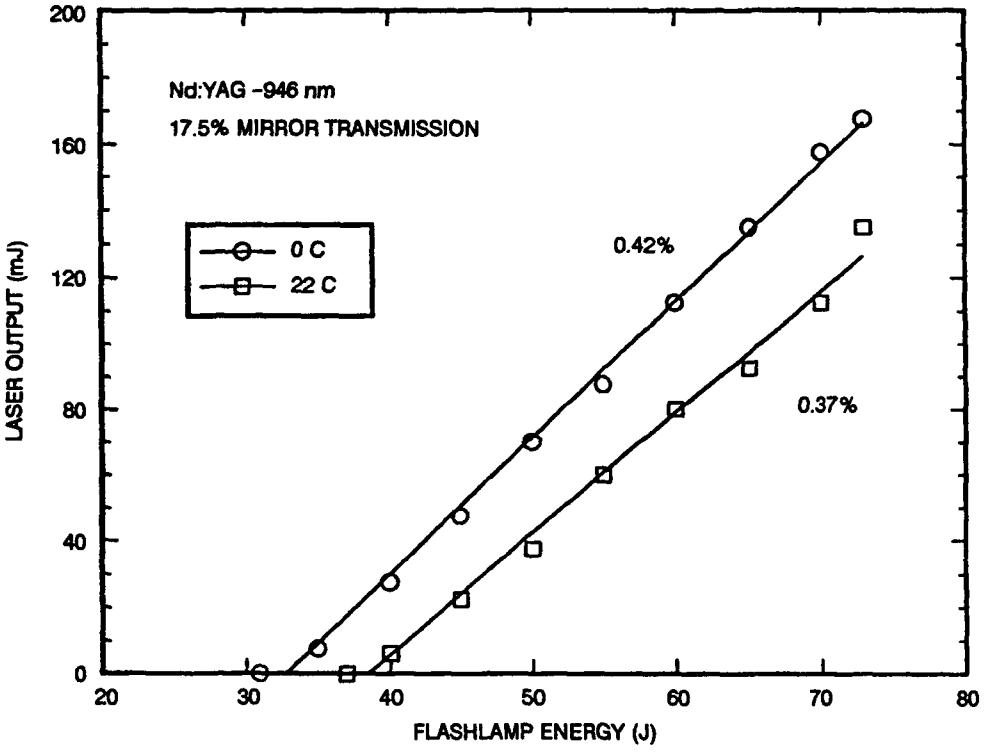

Figure 5. Laser output at 946 nm versus flashlamp energy.

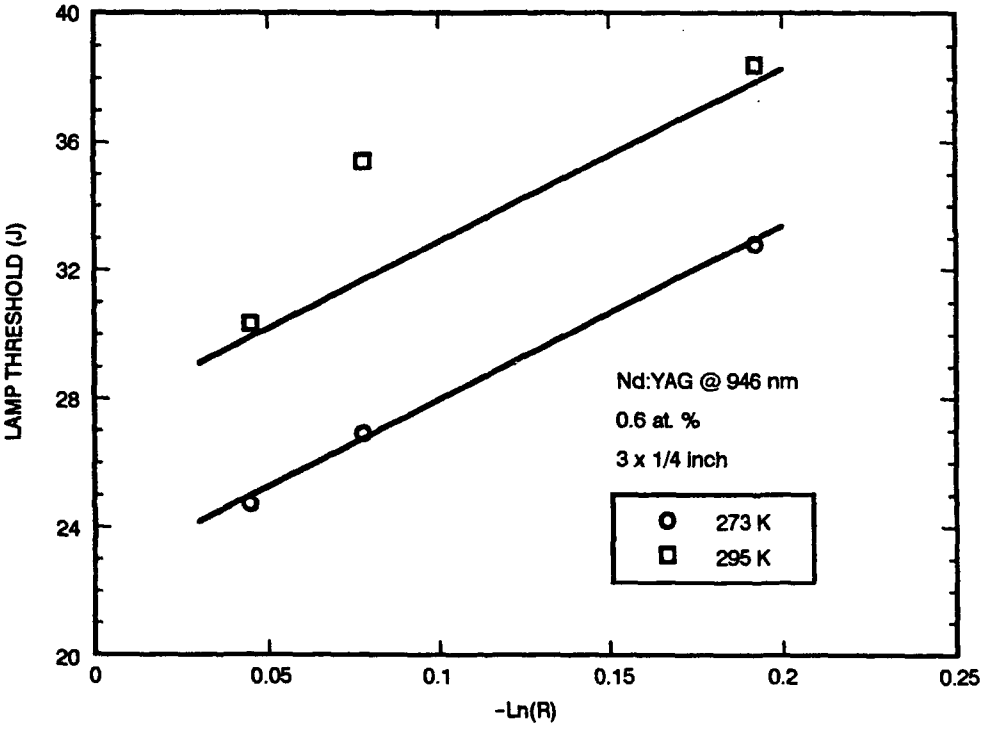

Figure 6. Laser threshold summary at 946 nm.

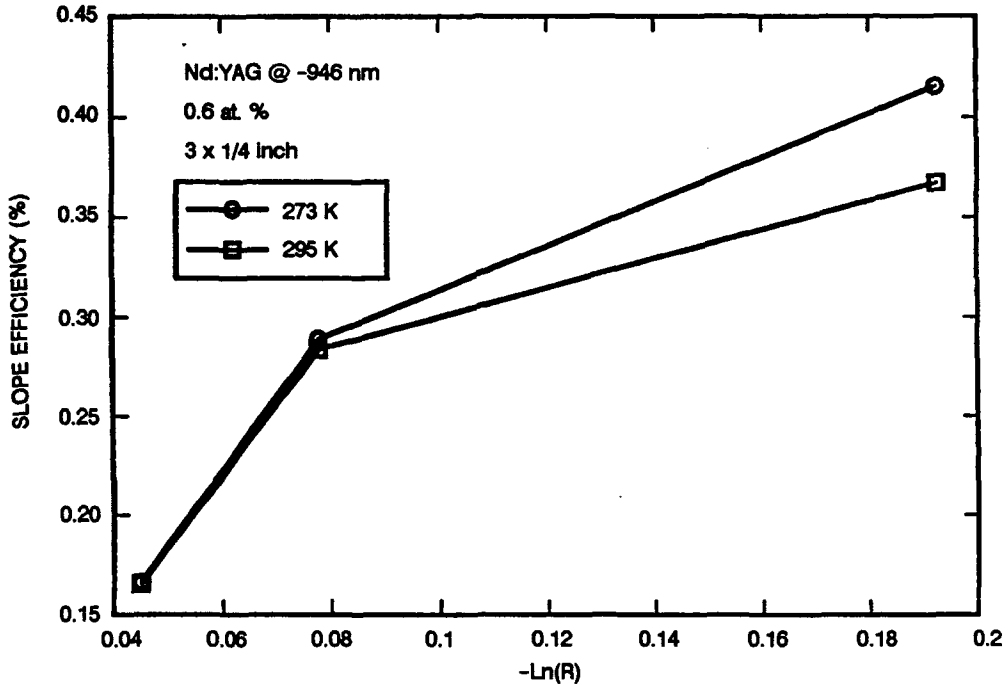

Figure 7. Laser slope efficiency summary at 946 nm.

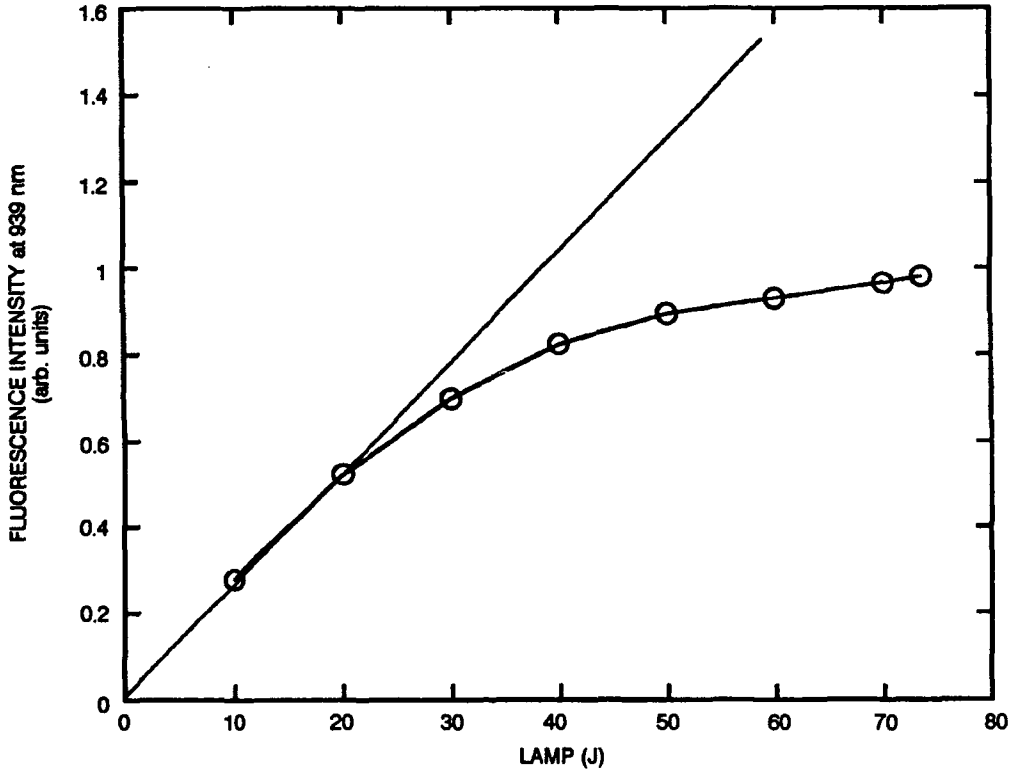

Figure 8. Fluorescence sidelight as a function of flashlamp energy.

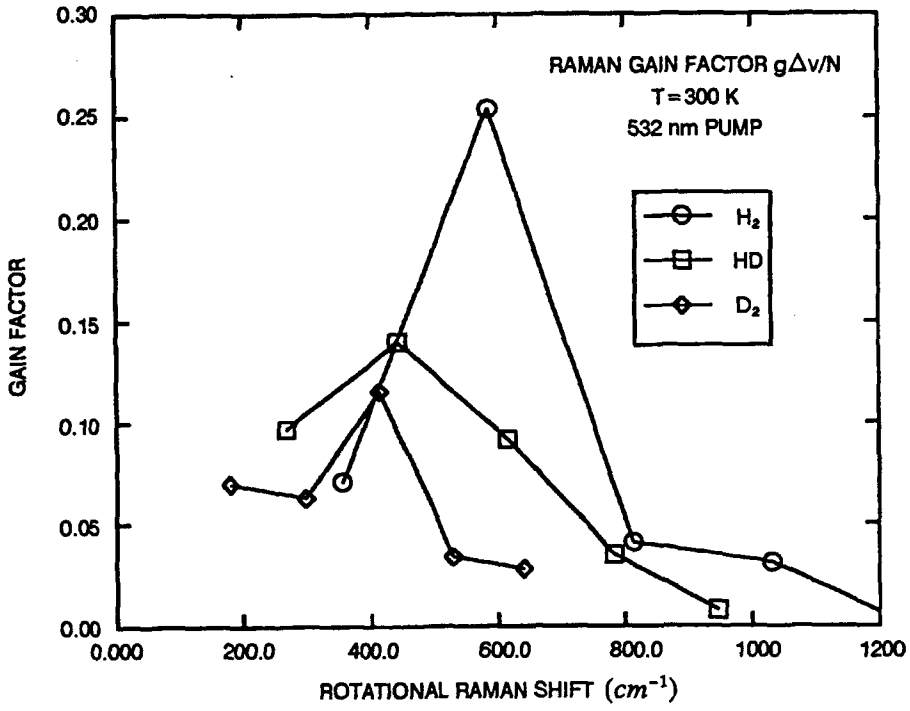

Figure 9. Calculated rotational Raman gain spectrum, gΔv/N, for hydrogen.

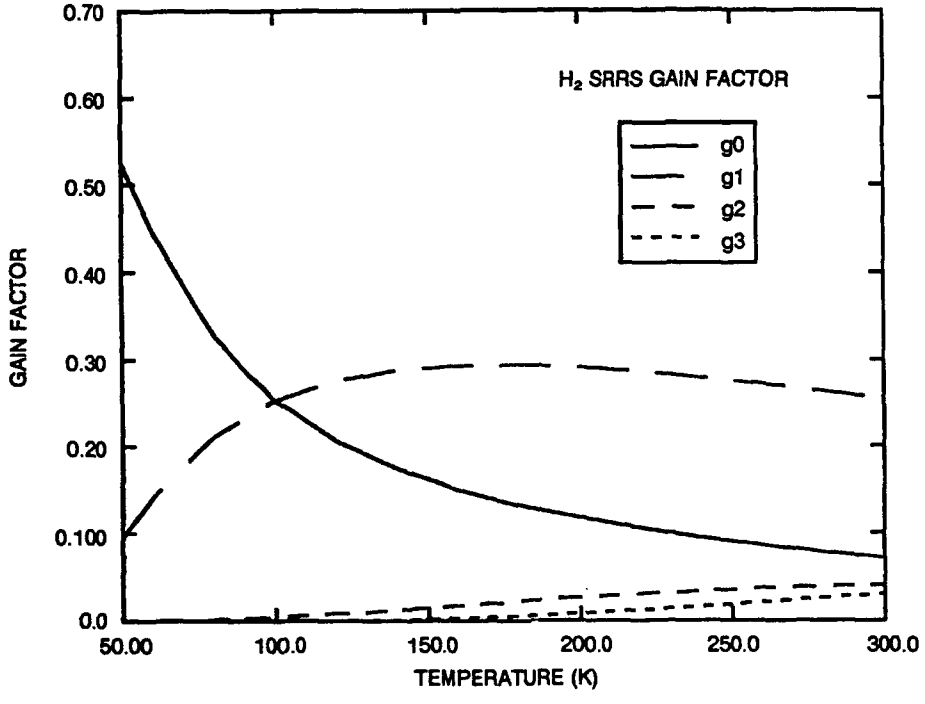

Figure 10. Temperature dependence of gain, gΔv/N, for H_2.

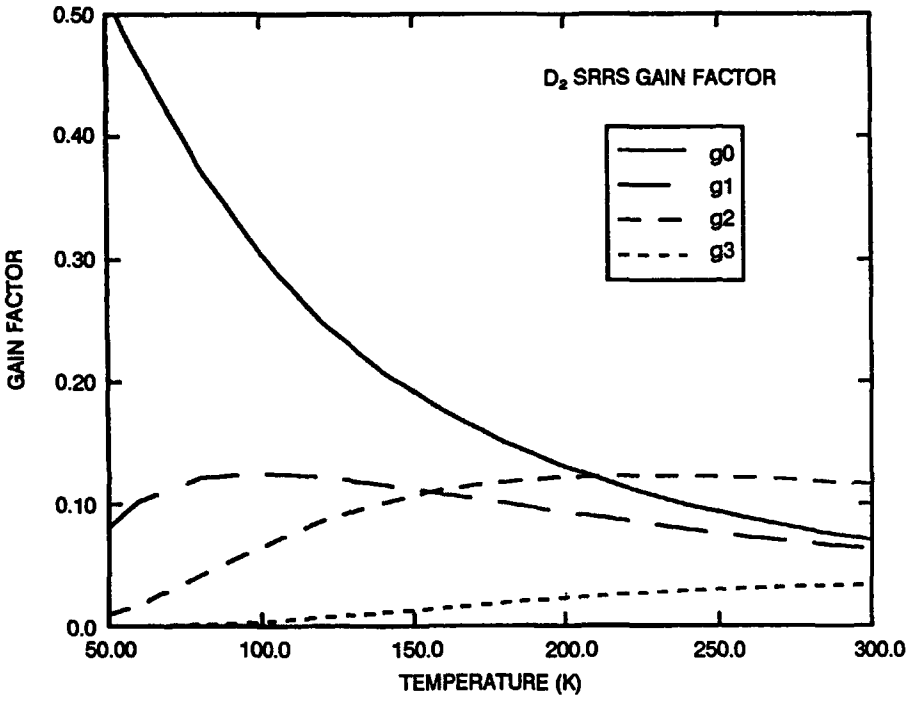

Figure 11. Temperature dependence of gain, $g\Delta v/N$, for D_2.

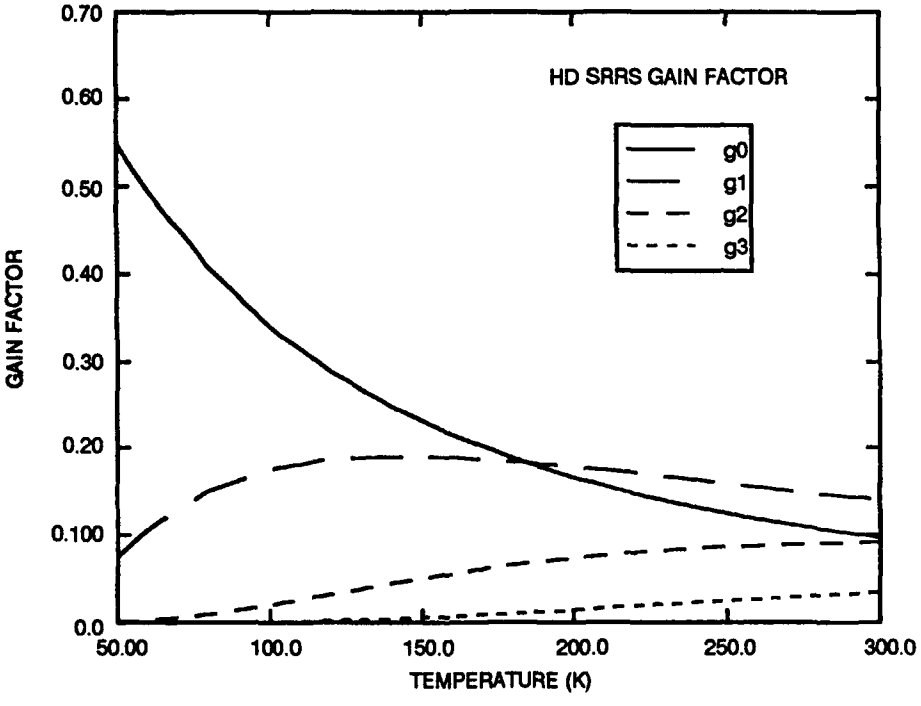

Figure 12. Temperature dependence of gain, $g\Delta v/N$, for HD.

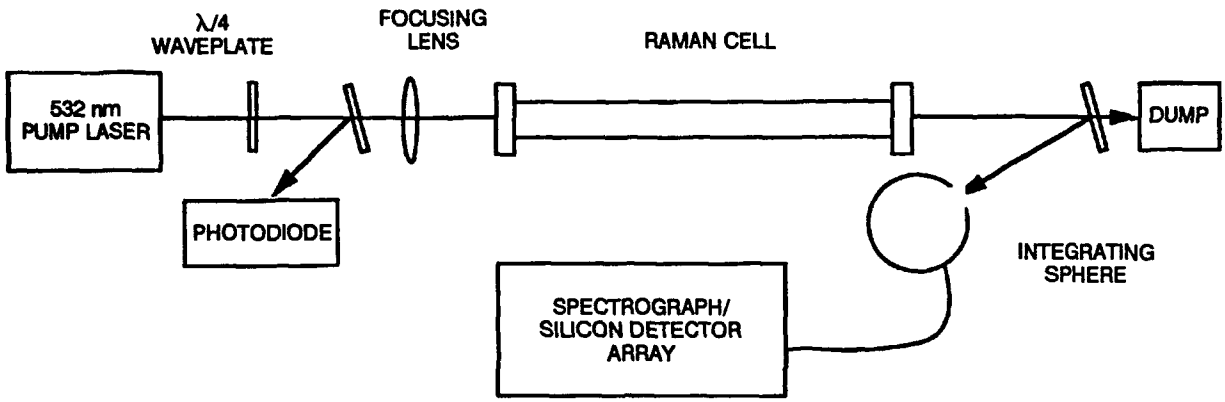

Figure 13. Experimental Raman setup.

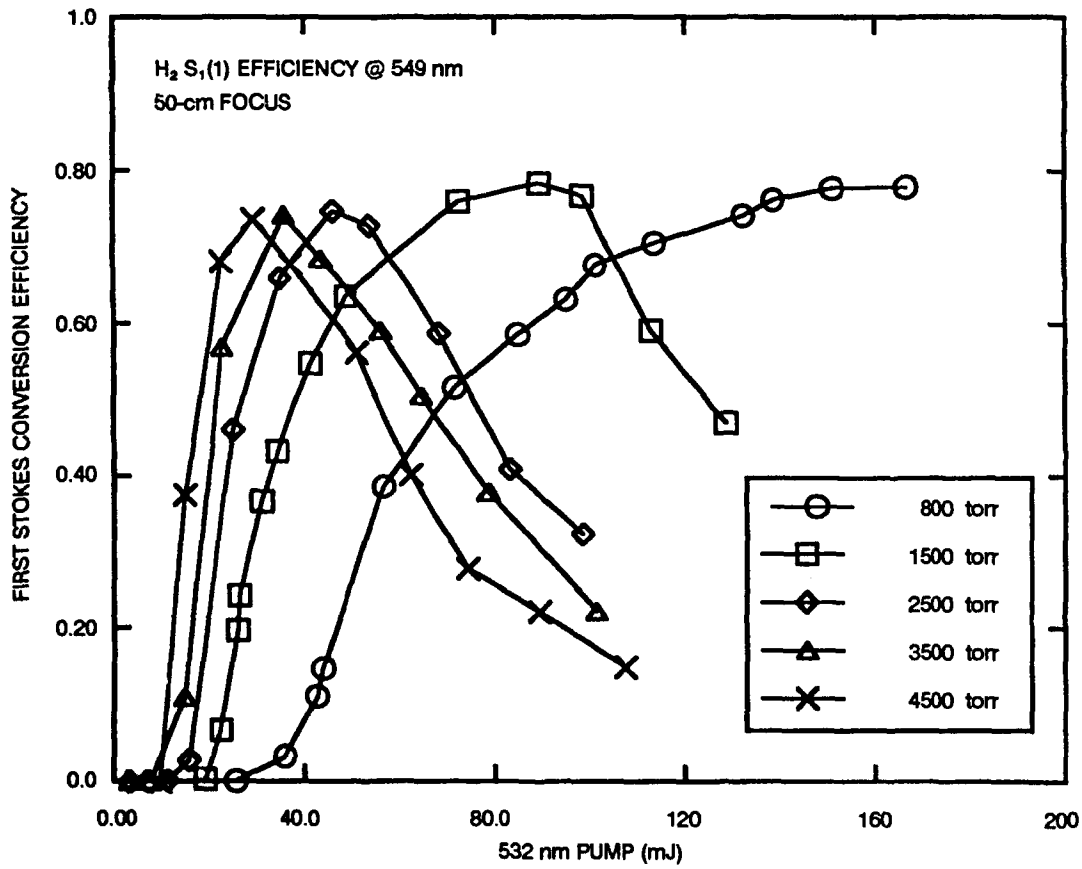

Figure 14. SRRS efficiency in H_2 with a 50-cm focusing lens.

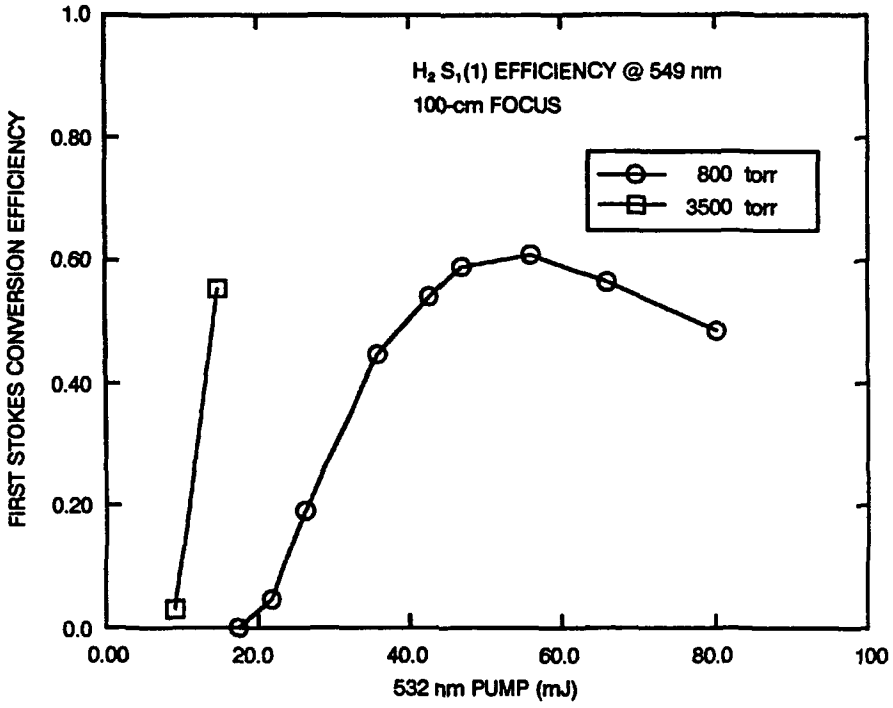

Figure 15. SRRS efficiency in H_2 100-cm focusing lens.

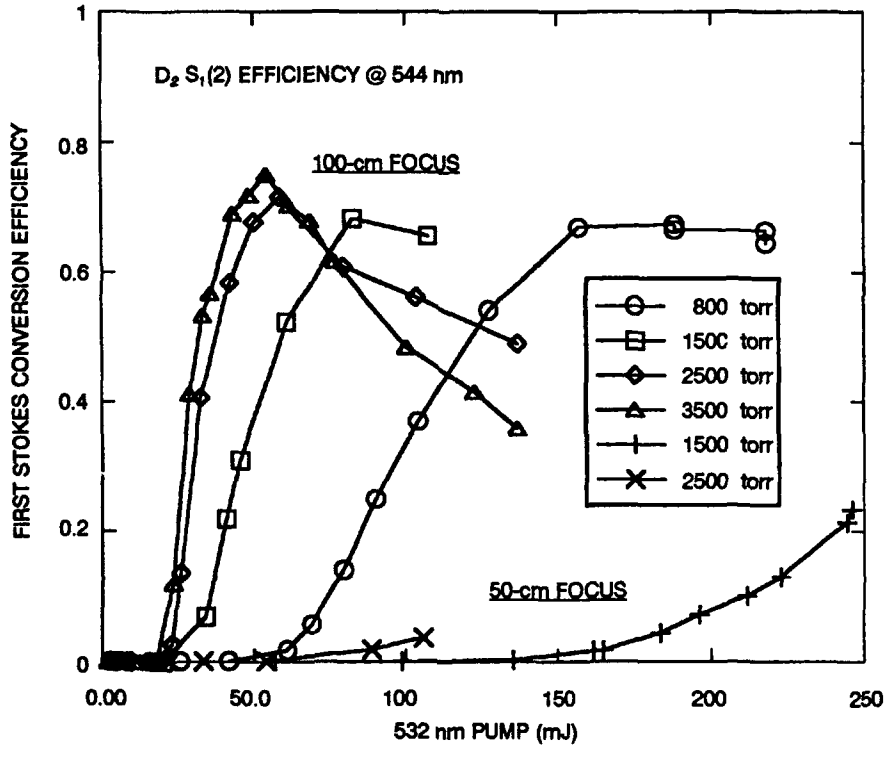

Figure 16. SRRS efficiency in D_2.

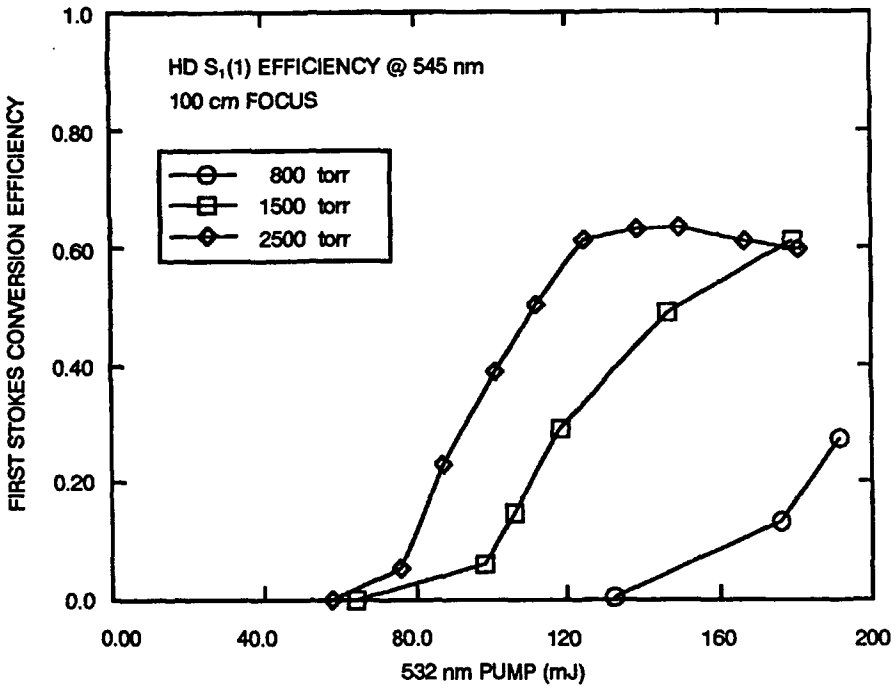

Figure 17. SRRS efficiency in HD.

REPORT DOCUMENTATION PAGE

Form Approved
OMB No. 0704-0188

1. AGENCY USE ONLY *(Leave blank)*	2. REPORT DATE	3. REPORT TYPE AND DATES COVERED
	March 1992	Final

4. TITLE AND SUBTITLE

FEASIBILITY OF A 486 nm FRAUNHOFER LASER SOURCE BASED ON A $^4F_{3/2} \rightarrow {}^4I_{9/2}$ NEODYMIUM LASER

5. FUNDING NUMBERS

PR: ZF07
PE: 0602936N
WU: RV36121

6. AUTHOR(S)

F. E. Hanson, D. L. Katz and P. Poirier

7. PERFORMING ORGANIZATION NAME(S) AND ADDRESS(ES)

Naval Command, Control and Ocean Surveillance Center (NCCOSC),
RDT&E Division (NRaD)
San Diego, CA 92152-5000

8. PERFORMING ORGANIZATION REPORT NUMBER

NRaD TR 1480

9. SPONSORING/MONITORING AGENCY NAME(S) AND ADDRESS(ES)

Office of Chief of Naval Research
Independent Exploratory Development Programs (IED)
OCN-20T
Arlington, VA 22217

10. SPONSORING/MONITORING AGENCY REPORT NUMBER

11. SUPPLEMENTARY NOTES

12a. DISTRIBUTION/AVAILABILITY STATEMENT

Approved for public release; distribution is unlimited.

12b. DISTRIBUTION CODE

13. ABSTRACT *(Maximum 200 words)*

Investigate the potential of a novel laser source based on the neodymium $^4F_{3/2} \rightarrow {}^4I_{9/2}$ transition for operation at 486.1 nm, the H_β Fraunhofer wavelength. Characterize this transition in Nd:YAG and also stimulated rotational Raman conversion in H_2, D_2, and HD as critical steps in such a system.

14. SUBJECT TERMS

lasers
optics
nonlinear optics

15. NUMBER OF PAGES

27

16. PRICE CODE

17. SECURITY CLASSIFICATION OF REPORT	18. SECURITY CLASSIFICATION OF THIS PAGE	19. SECURITY CLASSIFICATION OF ABSTRACT	20. LIMITATION OF ABSTRACT
UNCLASSIFIED	UNCLASSIFIED	UNCLASSIFIED	SAME AS REPORT

21a. NAME OF RESPONSIBLE INDIVIDUAL	21b. TELEPHONE *(Include Area Code)*	21c. OFFICE SYMBOL
F. E. Hanson	(619) 553–5720	Code 843

INITIAL DISTRIBUTION

Code 0012	Patent Counsel	(1)
Code 0142	K. Campbell	(1)
Code 0144	R. November	(1)
Code 144	V. Ware	(1)
Code 80	K. D. Regan	(1)
Code 804	E. Schimitschek	(1)
Code 804	G. Beaghler	(1)
Code 84	M. S. Kvigne	(1)
Code 843	D. M. Gookin	(1)
Code 843	D. Katz	(1)
Code 843	P. Poirier	(1)
Code 843	F. Hanson	(12)
Code 952B	J. Puleo	(1)
Code 961	Archive/Stock	(6)
Code 964B	Library	(2)

Defense Technical Information Center
Alexandria, VA 22304-6145 (4)

NCCOSC Washington Liaison Office
Washington, DC 20363-5100

Center for Naval Analyses
Alexandria, VA 22302-0268

Navy Acquisition, Research & Development
Information Center (NARDIC)
Alexandria, VA 22333

Naval Command, Control & Ocean
Surveillance Center
RDT&E Division Detachment
Warminster, PA 18974-5000 (2)